Published as:
Physics of Plasmas **30**, 062303 (2023)
doi:10.1063/5.0146229

Intrinsic Evolution of the Decoupling and Coupling of the plasma Density and Temperature in a Cylindrical Laboratory Plasma Device

C.Y. Wang[1], W. W. Xiao[1*], Y. Ren[2], P.H. Diamond[3], X.B. Peng[4], J.T. Ma[1], W.J. Zhong[1]

1 Institute for Fusion Theory and Simulation, School of Physics, Zhejiang University, Hangzhou, 310027, China
2 PPPL, Princeton University, P.O. Box 451, Princeton, New Jersey 08543, USA
3 Center for Energy Research, University of California San Diego, La Jolla, CA 92093, USA
4 Institute of Plasma Physics, Chinese Academy of Sciences, Hefei Anhui, 230031, China

Email: wwxiao@zju.edu.cn

Abstract

An intrinsic evolution on the decoupling-coupling-decoupling (DCD) of the electron density and temperature responding to the magnetic field change is observed in a cylindrical laboratory plasma device. Experimental results show that the density and the temperature decouple in low magnetic field, couple with higher magnetic field and decouple again with continuous magnetic field increase. An element physical picture of the DCD regime is unraveled based on the analyses of gradient lengths, the turbulence propagation directions and the turbulence spatial scales, and the relationship between the normalized collision rates and the poloidal mode numbers.

I. Introduction

Since sawtooth oscillation was firstly observed [1] in magnetically confinement fusion (MCF) field, the physics of the coupling and the decoupling has been studied for several decades [2-6]. The coupling and the decoupling between the density profiles and the temperature are extensive and important physical phenomena in magnetized plasma. Typically, the density profiles and the temperature profiles are generally reported on the high confinement mode (H-mode) [7-9] and the improved energy confinement mode (I-mode) [10-13] in the tokamak edge region.

In this work, we report an intrinsic evolution of the decoupling-coupling-decoupling (DCD) based on the gradient changes of the density and the temperature in the ZPED.

Here, the "coupling" means that the gradients of the density and the temperature change synchronously, the "decoupling" means that the density gradient and the temperature gradient change asynchronously or reversely change. The distinct physics on the intrinsic evolution of the decoupling and coupling of the plasma density and temperature was discussed from three aspects in this paper. *First,* the temperature gradient almost does not change while the density gradient increases with the magnetic field increase from 0.5 kGs to 0.8 kGs. This means that the decoupling phenomenon exists due to the asynchronous change of the gradients in region I. Then the density gradient and the temperature gradient synchronously increase with the magnetic field increase from 0.8 kGs to 1.1 kGs. This is so-called the coupling phenomenon in region II. And then the density gradient almost does not change while the temperature gradient continuously increases with the magnetic field increase from 1.1 kGs to 2 kGs. We call the density and the temperature are decoupled in region III. *Second,* the propagation directions of the poloidal wavenumber (k_θ) and the radial wavenumber (k_r) with magnetic field changes, and the drift wave (DW) [14] extends to higher frequency region. *Third,* the density gradients drive a nonlinear change of the density fluctuations with magnetic field increase, and the integral density decreases but the integral temperature increases. Meanwhile, the relationship between the normalized collision rates of the electron to electron (v_{ee}^*) and the poloidal mode numbers (m) at r=4.5cm is strongly related to the density. This means that one potential mechanism affects density, which is the driven source of the DCD regime in this experiment. Finally, we discussed the H-mode and I-mode plasmas on the v_{ee}^* and the m based on a few tokamak experiments. A comparison shows that the intrinsic evolution of the DCD phenomenon is similar to the edge gradient changes between the H-mode and the I-mode plasmas. The density could be one of the key parameters associated with the transfer between the H-mode and I-mode.

II. Experiment setup

The experiments reported were carried on the Zheda Plasma Experimental Device (ZPED) [15], which is a cylindrical magnetized plasma device at Zhejiang University,

as shown in figure 1. The figure 1 (a) is the picture of the real device and figure 1 (b) is the schematic diagram of the ZPED. The size of the vacuum chamber is 2.0m in length and 0.3m in diameter. The Nitrogen plasma is produced by a 13.56MHz radio frequency (RF) source with about 200W forward and about 20W reflect power. The *A* to the *G* represent the RF source, the vacuum chamber, the magnetic coils, the diagnostic window for the microwave reflectometry, the throttle valve and pump system, the glass observation window and the cooling water tubes, respectively. The coil thick is 94 mm as shown in figure 1 H. The gas fueling system is located at the head of vacuum chamber, as shown by the yellow arrow. The Quadruple Langmuir probe (QLP) [16] and the Langmuir rake probes are the key diagnostics for the density and temperature profiles, the density fluctuations in this experiment. The sampling frequency of the QLP and the Langmuir rake Langmuir probes is 2MHz. The locations of the QLP and the Langmuir rake probes are marked by the red arrows in the figure 1 (a) and (b). A camera is localized at the end of the device for the observation of the poloidal mode numbers (m).

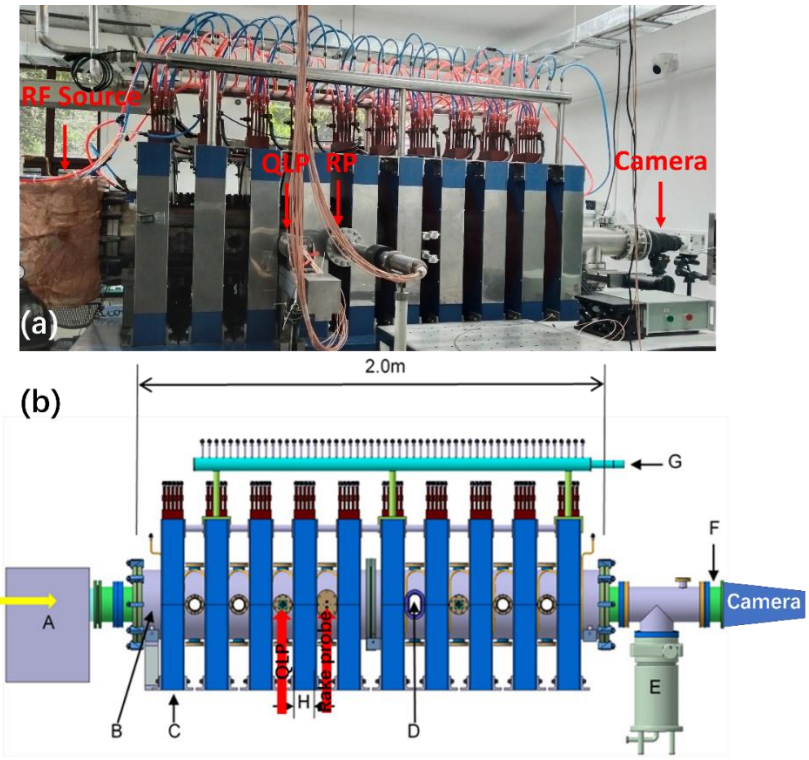

FIG. 1 (a) is the real device picture and (b) is the schematic diagram of the ZPED [17]. The locations of the Quadruple Langmuir probe (QLP) and the Langmuir rake probes are marked by the red arrows. A camera is localized at the end of the device for the observation of the poloidal mode numbers (m).

The detailed structures and directions of the QLP and the Langmuir rake probes are shown in figure 2. The diagram of QLP is shown in figure 2 (a). It consists of four tungsten tips, 1, 2, 3 and 4 of 1cm in length and 1.4mm in diameter. The distance between the tip3 and the tip4 along the poloidal direction is 4.6 mm and the distance between the tip1 and tip2 along the magnetic field direction is 4.5 mm, as shown in Figure 2 (a). The plasma profiles (electron density, electron temperature), the density fluctuations and the poloidal wavenumbers (k_θ) are measured by the QLP. The diagram of the Langmuir rake probe is shown in Figure 2 (b). It consists of 12 tungsten tips in the radial direction from the center to the edge. The length and the diameter of each tip are 2mm and 2mm, respectively. The distance between two adjacent tips is 4mm. The radial wavenumbers (k_r) can be measured by the Langmuir rake probe. The magnetic field direction and the moving direction of the QLP and the Langmuir rake probe are marked by the arrows in Figure 2. In the experiment, a passive RF compensation circuit is connected just after the probe tip. The detailed parameters of each probe tip are: the capacitance is 20pF and the inductance is 6.8μH. The main purpose of the RF compensation circuit is to eliminate the influence of the 13.56MHz RF signal from the RF source [18]. In this work, all of the poloidal mode numbers (m) can be observed by the fast camera diagnostic, which includes a high-speed camera and a lens system, as shown in figure 1. The camera parameters are the spatial resolution of 512*512, frames per second of 24000 and the exposure time of 10μs. The details on the fast camera diagnostic was studied in [19].

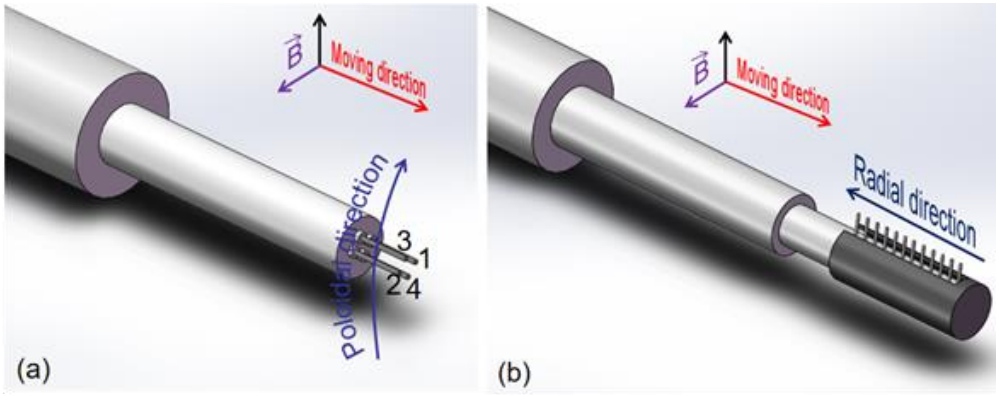

FIG. 2 (a) is the diagram of QLP and (b) is the diagram of Langmuir rake probe. The magnetic field direction, the poloidal direction and the moving direction are indicated by the arrows.

III. Experimental results and analysis

A. The measurements of the density and the temperature

The density profiles and the temperature profiles with different magnetic fields are measured by the QLP as shown in Figure 3 (a) and (b), respectively. Actually, in order to measure the profiles of the density and the temperature, we used the reciprocating motion method to get the raw data. It means that the QLP system is driven by an electric motor, which is controlled by the software as experiment needed, such as the swept velocity and the depth in the plasma. In figure 3, the numbers of each global profile of the density and the temperature is about 2×10^5 along the radial direction, and the representative points with the error bars on the profiles are to avoid the curves of the profiles overlap each other.

However, the ionization of the gas in the linear machine is non-negligible issue because there is no extra heating source except the RF source. Thus, the plasma temperature decreases from the head to the rear of the device. In order to get good plasma performance on the ZPED, the optimized detection positions of the QLP and the Langmuir rake probe are considered to avoid the RF source influence and the plasma temperature drop. The distance between the RF source and the probes is about 80-100cm, as shown in figure 1 by the red arrows. In addition, we chose a special region of the plasma, as shown in figure 3 by the shaded bars. The turbulence and the incomplete ionization in the plasma edge are the main reasons for the measurement errors of the Langmuir probe system. Meanwhile, in the core region of the linear machine, the hollow profiles of the density and temperature are often observed in linear machines, a most possibility is also the incomplete ionization in the core region of a linear device. Thus, we chose the special region to study, as shown in figure 3 by the shaded bars.

A local ionization of the gas is estimated using the Saha equation [20, 21] $a^2/(1-a^2)=(2.4\times10^{-4}/p)T^{2.5}e^{-u/KT}$. The main analysis region of the local ionization of the gas is at r~4.5cm (as shown by the red lines in figure 3). Then, the local ionization of the gas could be estimated. The local ionization number a is about 99% at the local

measurement position only, r~4.5cm. Here, the T represents the thermodynamic temperature, ~ 3×10^4 K, the ionization energy (u) of nitrogen atom is 14.5 eV, the plasma temperature (KT) is about 3eV, and the pressure (p) is about 1.5mtorr, which was measured by the vacuum gauge in the ZPED. Note: the local ionization of the gas does not imply the global ionization because the recombination rate of the electron-ion will increase as long as it is far from the RF source in a linear machine without extra heating source, and the global ionization of low temperature plasma using the Saha equation should be studied based on more special experiments or using a coronal model estimate for the globe ionization balance due to the complex atomic molecular physics processes.

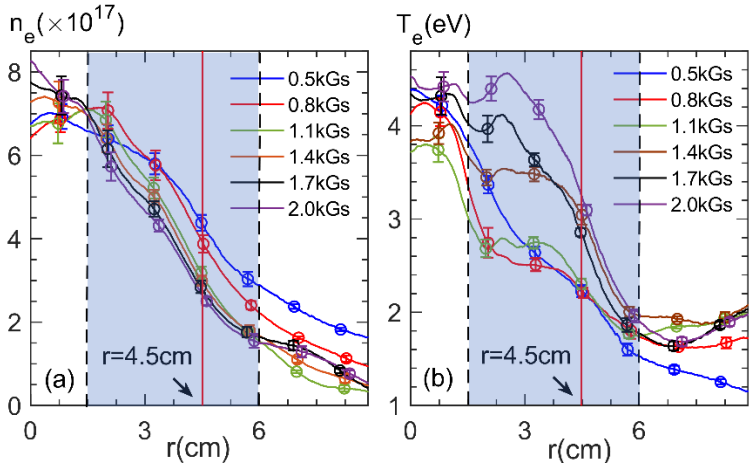

FIG. 3 (a) and (b) are the density profiles and the temperature profiles, respectively. The main analysis region is at r=4.5cm, as shown by the red line. The regions of the integral density and the integral temperature are represented by the shaded bars, which are confirmed by the black dashed lines. Corresponding to the integral density and the integral temperature will be discussed in section III D.

B. The density gradient evolution with different magnetic fields

Based on Figure 3, a detailed analysis of the gradient is shown in Figure 4. The density gradient length ($1/L_{ne}= \Delta n_e/ n_e$) and the temperature gradient length ($1/L_{Te}= \Delta T_e/ T_e$) are shown by the blue curve and the red curve, respectively. The density gradient increases with the magnetic field increase, while the temperature gradient almost does not change even the magnetic fields increase, as shown in figure 4 in the region I. The density gradient continuously increases, meanwhile the temperature gradient increases with the magnetic increase as well in region II; however, the temperature gradient increases with

the magnetic field increase but the density gradient almost does not change in region III. These results indicate that the DCD regime exists with the magnetic field increase:

(1) the density profile and the temperature profile are decoupled in region I, density gradient increases while the temperature gradient almost does not change;

(2) the density and the temperature are coupled in region II, both the density gradient and the temperature gradient increase synergistically;

(3) the density and the temperature are decoupled, the temperature gradient increases while the density gradient does not change in region III.

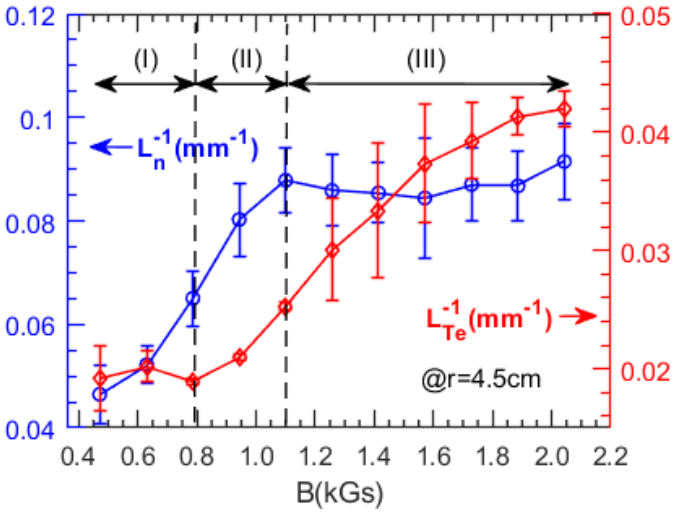

FIG. 4 the distributions of the $1/L_n$ and the $1/L_{Te}$ at r=4.5cm with magnetic field change. The three regions of the DCD regime are separated by the gradient changes of the density and the temperature.

C. The analysis of the wavenumber spectra and the density fluctuation

In each region, the fundamental physics of the DCD regime related to the wavenumber spectra, the density fluctuation are analyzed, as shown in figure 5. The poloidal and the radial wavenumber spectra are obtained according to the two-point correlation method [22, 23], and the cross power spectra of floating voltage measured by two floating probes are derived with $C_{XY}^j = X^j(f)Y^{j*}(f) = Ae^{i\cdot\theta_j(f)}$, where j is the number of samples, X and Y are the Fourier transform of floating voltage, the star "*" denotes the complex conjugation. The wavenumber k_j is confirmed by the phase difference θ_j, $k_j(f) = \theta_j(f)/\Delta d$. By sum up complex amplitude of different samples, wavenumber spectra $S(k,f)$ can be calculated, $S(k,f) = \frac{1}{M}\sum_{j=1}^{M} I_{(0,\Delta k)}[k - k^j(f)] \cdot \left|C_{XY}^j(f)\right|$. Thus,

the wavenumber–frequency spectra S(k, f) of potential fluctuations for radial position r=4.5cm in region I, II and III are shown in figure 5. Here, the (a), (b) and (c) represent the changes of the poloidal wavenumber (k_θ) in the region I, II and III, and the (d), (e) and (f) represent the changes of the radial wavenumber (k_r) in the region I, II and III.

In region I: in figure 5 (a) and (d), the m=1 at 0.5kGs, the k_θ is at ion diamagnetic direction (i-direction, the turbulence spatial scale $k_\theta \rho_S = k_\theta \frac{\sqrt{m_i T_e}}{eB} = k_\theta \frac{\sqrt{14\times1.66\times10^{-27}\times1.6\times10^{-19}T_e(eV)}}{1.6\times10^{-19}\cdot B} = 3.8\times10^{-4}\frac{k_\theta\sqrt{T_e(eV)}}{B}$ =0.69, B=0.5kGs, $|k_\theta| < 60\ m^{-1},\ T_e \approx 2.3eV,\ \rho_S = 0.0116m$), while the k_r is outward as shown in figure 5 (d), and the frequency of the DW turbulence is below 10kHz, as shown in figure 5 (a) and (d) by the blue dashed lines.

In region II: in figure 5 (b) and (e), the m increases to 2 at 1.0kGs, while the k_θ is at the electron diamagnetic direction (e-direction, the turbulence scale $k_\theta \rho_S = 0.5904 < 0.6$, B=1000Gs, $|k_\theta| < 110\ m^{-1},\ T_e \approx 2.4eV, \rho_S = 0.0054m$), while the k_r is outward as shown in figure 5 (e), and the frequency of the DW turbulence expands to higher frequency range as shown in figure 5 (b) and (d).

In region III: when the magnetic field continuously increases, the m increases to 4 at 1.7kGs, the DW turbulence gradually transfers from ion diamagnetic direction to the electron diamagnetic direction and the absolute value of wavenumbers are much larger than that in region I and II, as shown in figure 5 (c). While, the k_r indicates that the turbulence transport in the low frequency region is still inward but the higher frequency turbulence transport is outward much, as shown in figure 5 (f).

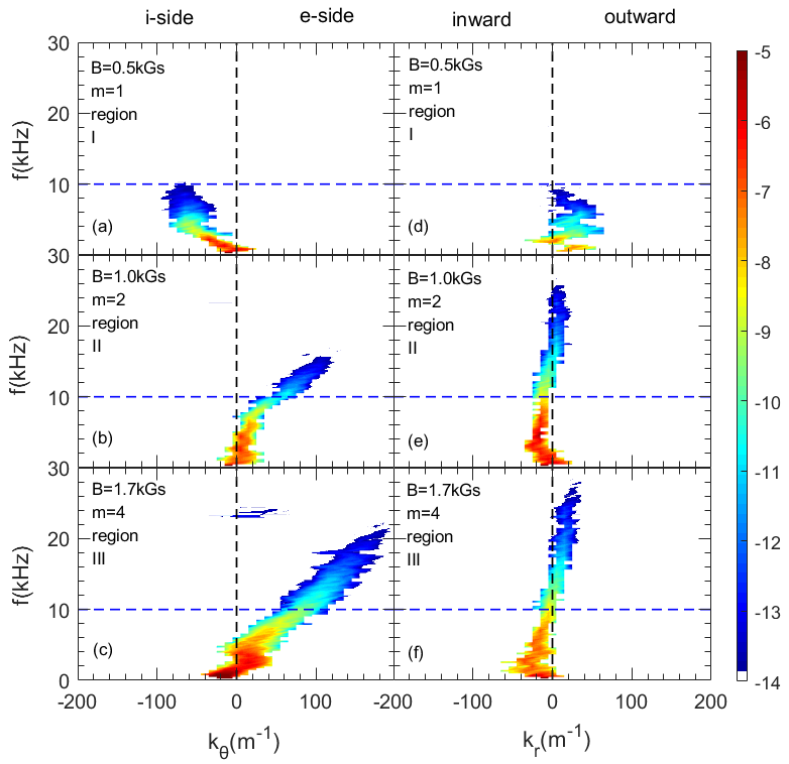

FIG. 5 Wavenumber–frequency spectra S(k, f) of the density fluctuations at r=4.5cm in region I, II and III. Here, the (a), (b), and (c) are the S(k_θ, f); the (d),(e) ad (f) are the S(k_r, f).

These results suggest that the low-frequency turbulence dominantly exists in low magnetic field. The turbulence propagation is at the ion diamagnetic direction. This is useful for the density increase since the diamagnetic effects as a finite pressure fluctuation to increase the total Reynolds force significantly [17]. While, with the magnetic field increase, the poloidal mode numbers increase from m=1 to m=4. It is clear that the turbulence frequency expands to a higher frequency and the turbulence propagation direction gradually reverses from i-side to e-side, as shown in figure 5 (b) and (c). The radial wavenumber spectra S(k_r, f) suggest that the turbulence frequency also increases, and the low frequency component of the turbulence is outward, as shown in figure 5 (d). In figure 5 (e) and (f), the higher frequency component of the turbulence is outward and the low frequency component of the turbulence reverses to inward direction. These results indicate that the drift wave turbulence with higher frequency could dominantly affect the particle confinement [24, 25]. The drift wave turbulence with higher frequency was driven by the magnetic field rising, as shown in figure 5 (c)

and (f). The particle confinement degradation is presented by the integral density decrease with the magnetic field increase, as shown in figure 6 (b).

Note: there is no clear difference between the regions II and III except the drift wave frequency increase. This indicates that there may be a coexisting status of the turbulence types from the region II to the region III. Actually, it is a little bit difficult to clearly separate the turbulence scales, the transport channels and the stabilization mechanisms [26]. Thus, it is better to specify the dominant characteristics in each region. Especially, in region III, the drift wave turbulence expands with the magnetic field increase and induces the confinement degradation. This is consistent with the drift wave turbulences occur universally in magnetized plasmas producing the dominant mechanism for the transport of particles [27].

D. The v_{ee}^{*} versus to the m

The turbulence saturation can be observed at the steep density gradient region when the magnetic field exceeds a critical magnetic field [28], which is defined due to the knee point of the density fluctuation curve, as shown in figure 6 (a) by the blue dashed line. Here, the fluctuation amplitude of the density is calculated from 4kHz to 20kHz at r=4.5cm, corresponding to the steep density gradient region in figure 3 by the red line. An integral density and temperature with different magnetic fields are also calculated, as shown in figure 6 (b). The integral regions are presented in figure 3 (a) and (b) by the black dashed lines, from r=1.5cm to 6cm in the ZPED. One can see that the integral density decreases, but the temperature increases with the magnetic field increase with no external particle, heating and momentum source. A possible reason is that the magnetic field leads to the increase of the DW turbulence amplitude and reduces the particle confinement, until to the turbulence amplitude saturation [29] in region III. This is consistent with the results in the figure 6 (b), the particle confinement dissipation with the increase of the DW turbulence, conversely, the temperature increases with the magnetic field increase. It suggests that an intrinsic evolution of the decoupling transport channel exists between the density and the temperature in a Cylindrical Laboratory Plasma Device with the magnetic field increase.

Thus, a relationship of the v_{ee}^{*} versus to the m is studied for a deep understanding of the intrinsic evolution of the DCD regime in this work, as shown in figure 6 (c). The v_{ee}^{*} related to the m at r=4.5 cm is calculated by the $v_{ee}^{*} = v/\omega_p,\ \omega_p = \sqrt{\frac{4\pi n_e e^2}{m_e}}$ as shown in figure 6 (c) [30]. Here, the v_{ee}^{*} is the normalized collision rate of the electron to electron, v is the collision rate by the $v = 2.91 \times 10^{-6} n_e \, ln\Lambda \, T_e^{-3/2} s^{-1}$ and the $ln\Lambda = 23 - ln(n_e^{\frac{1}{2}} T_e^{-\frac{3}{2}})$ at $T_e \leq 10eV$, the ω_p is the plasma frequency, the n_e is the plasma density, the e is the electronic charge and the m_e is the electron mass, respectively. A change trend of the v_{ee}^{*} versus to the m in the three regions is shown in figure 6 (c) by the dotted ellipses. The v_{ee}^{*} does not change while the m increases in figure 6 (c) region I, and the m stops increasing in figure 6 (c) in region II, and the m is almost saturated and the v_{ee}^{*} decreases in figure 6 (c) region III. These suggest that the low density due to the turbulence dissipation is one of the key points of the intrinsic evolution on the DCD regime of the density and the temperature.

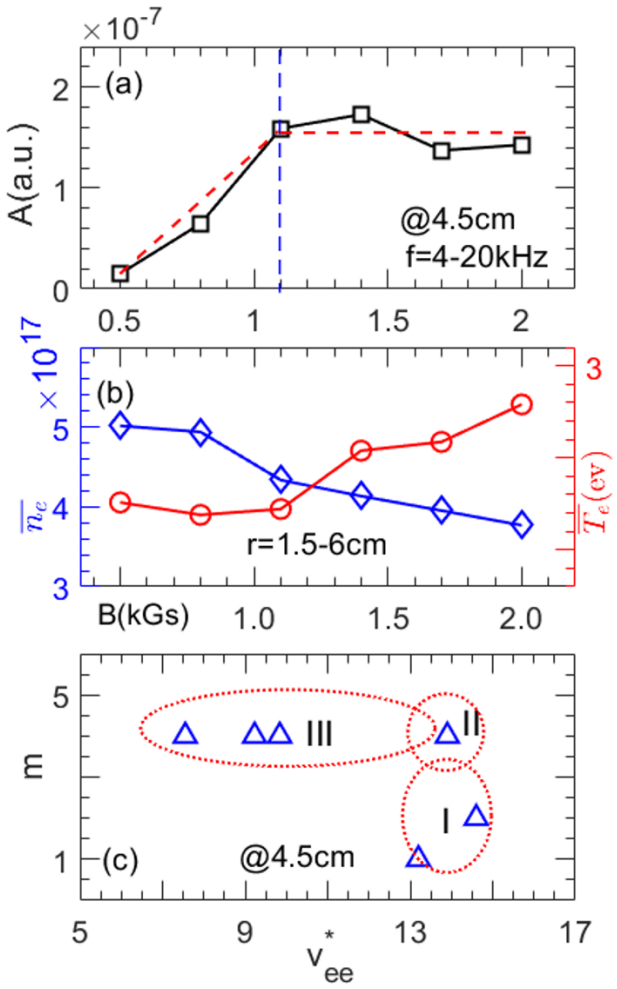

FIG. 6 (a) is the amplitudes of the density fluctuation with different magnetic fields, the critical magnetic field is pointed by the blue dashed line. (b) shows the integral density and the integral temperature and the integral radius r is from 1.5 cm to 6cm. (c) represents the relationship between the v_{ee}^{*} *and the* m.

IV. Discussion and summary

Actually, a few typical results on the v_{ee}^{*} versus to the m related to the H-mode and I-mode plasmas from different machines are statistically evaluated in the plasma edge region at ρ=0.95, as shown in figure 7. The data points are based on the experimental results from DIII-D, EAST, ASDEX-U and C-MOD. The red stars and the red circles represent the H-mode and the I-mode plasmas with different densities, respectively. The table 1 shows the v_{ee}^{*}, the m and the $< n_e >$. It is clear that the H-mode plasma density is larger than that in the I-mode case based on the data in the table 1. A regular shape of the v_{ee}^{*} versus to the m is almost similar to the results in figure 6 (c). A comparison between the figure 7 and the figure 6 (c) indicates that the density is a key

parameter to induce the intrinsic evolution of the DCD regime, and this may be helpful to understand the different transport channels of the density and the temperature in the H-mode and the I-mode plasmas [31].

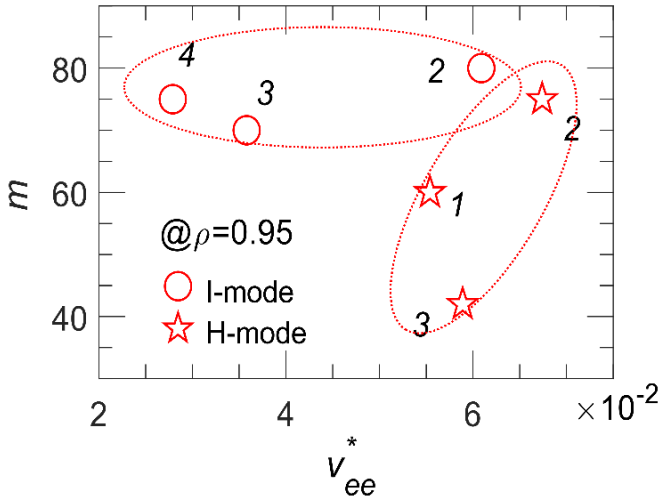

FIG. 7. The relationship between the v_{ee}^{*} and the m. The numbers 1-4 correspond to the data from the tokamaks DIII-D, EAST, ASDEX-U and C-MOD. The red stars and the red circles represent the H-mode and the I-mode plasmas with different densities, respectively. The details are shown in Table 1.

Table 1: the details of the v_{ee}^{*}($\times 10^{-2}$), the m and the $< n_e >$($\times 10^{19} m^{-3}$) from a few tokamaks with H-mode and I-mode plasmas.

		DIII-D	EAST	ASDEX-U	C-MOD
v_{ee}^{*}	H	5.54[31]	6.74[32]	2.83[31, 33]	5.89[31]
	I	7.34[31]	6.09[34]	2.79[31, 33]	3.58[12, 31]
m	H	60[35]	75[36-38]	40[39, 40]	42[41, 42]
	I	~70[12, 43]	~75[34]	75[44]	~70[12]
<ne>	H	5.5[45]	3[37]	~5.0[46, 47]	~26[48]
	I	4.5[12]	~2.5[38]	~3.5[33]	~12[49]

In general, an intrinsic evolution on the DCD regime has been observed on ZPED with the magnetic field increase: *first*, the temperature gradient almost did not change while the density gradient increased in region I, and this phenomenon is called decoupling between the density and the temperature; *second*, both density and temperature gradient increased synergistically in region II, and this phenomenon is called coupling between the density and the temperature; *third*, the density gradient almost did not change while the temperature gradient continuously increased with the magnetic field increase in region III, and this is called decoupling again between the density and the temperature.

In addition, with the magnetic field increase, the turbulence propagation direction gradually reversed and the DW turbulence frequency expanded to higher frequency region with higher wavenumber. The DW turbulence dominantly reduced the density and degraded particle confinement, which is the element point to change the density. A regular shape of the v_{ee}^{*} versus to the m identifies that the density is a key parameter of the intrinsic evolution on the DCD regime in the cylindrical laboratory plasma.

How to confirm a global plasma ionization in a linear machine with about 5 eV and a density less than 10^{18} m^{-3} could be a new direction to study, even the Saha equation might be applied to explain a local ionization in low temperature plasma in this paper. However, this conclusion of the local ionization using Saha is possible a reference only [50, 51]. Thus, it would be more appropriate to use a coronal model estimate for the ionization balance in the linear machine plasma. A valuable research direction on this point will be focused in the next experimental studies.

Acknowledgments

The authors thank J.Q. Dong, X.T. Ding, G.R. Tynan, X.L. Zou for many enlightening discussions. This work was supported by the National Natural Science Foundation of China (Grant No.11875234) and the National Magnetic Confinement Fusion Science Program of China (2017YFE0301206, 2017YFE0300500 and 2017YFE0301200).

Data availability

The data that support the findings of this study are available from the corresponding author upon reasonable request.

References:

[1] J. D. Callen and G. L. Jahns, “Experimental measurement of electron heat diffusivity in a tokamak,” Phys. Rev. Lett. 38, 491–494 (1977).

[2] D. L. Brower, C. X. Yu, R. V. Bravenec, H. Lin, N. C. Luhmann, W. A. Peebles, C. P. Ritz, B. A. Smith, A. J. Wootton, Z. M. Zhang, and S. J. Zhao, “Confinement degradation and enhanced microturbulence as longtime precursors to high-density-limit tokamak disruptions,” Phys. Rev. Lett. 67, 200–203 (1991).

[3] G. M. D. Hogeweij, J. O'Rourke, and A. C. C. Sips, "Evidence of coupling of thermal and particle transport from heat and density pulse measurements in jet," Plasma Phys. Control. Fusion 33, 189 (1991).
[4] N. Deliyanakis, D. P. O'Brien, B. Balet, C. M. Greenfield, L. Porte, A. C. C. Sips, P. M. Stubberfield, and H. Wilson, "The VH-mode at JET," Plasma Phys. Control. Fusion 36, 1159 (1994).
[5] C. Hidalgo, B. Gonçalves, C. Silva, M. A. Pedrosa, K. Erents, M. Hron, and G. F. Matthews, "Experimental investigation of dynamical coupling between turbulent transport and parallel flows in the jet plasma-boundary region," Phys. Rev. Lett. 91, 065001 (2003).
[6] G. R. Tynan, R. A. Moyer, M. J. Burin, and C. Holland, "On the nonlinear turbulent dynamics of shear-flow decorrelation and zonal flow generation," Phys. Plasmas 8, 2691–2699 (2001).
[7] F. Wagner, G. Fussmann, T. Grave, M. Keilhacker, M. Kornherr, K. Lackner, K. McCormick, E. R. Müller, A. Stäbler, G. Becker, K. Bernhardi, U. Ditte, A. Eberhagen, O. Gehre, J. Gernhardt, G. v. Gierke, E. Glock, O. Gruber, G. Haas, M. Hesse, G. Janeschitz, F. Karger, S. Kissel, O. Klüber, G. Lisitano, H. M. Mayer, D. Meisel, V. Mertens, H. Murmann, W. Poschenrieder, H. Rapp, H. Röhr, F. Ryter, F. Schneider, G. Siller, P. Smeulders, F. Söldner, E. Speth, K. H. Steuer, Z. Szymanski, and O. Vollmer, "Development of an edge transport barrier at the h-mode transition of asdex," Phys. Rev. Lett. 53, 1453–1456 (1984).
[8] D. P. Schissel, M. A. Mahdavi, J. C. DeBoo, and M. Le, "Decoupling the effects of plasma current and plasma density on DIII-D H mode energy confinement," Nucl. Fusion 34, 1401 (1994).
[9] D. G. Whyte, A. E. Hubbard, J. W. Hughes, B. Lipschultz, J. E. Rice, E. S. Marmar, M. Greenwald, I. Cziegler, A. Dominguez, T. Golfinopoulos, N. Howard, L. Lin, R. M. McDermott, M. Porkolab, M. L. Reinke, J. Terry, N. Tsujii, S. Wolfe, S. Wukitch, Y. Lin, and t. A. C.-M. Team, "I-mode: an H-mode energy confinement regime with L-mode particle transport in Alcator C-Mod," Nucl. Fusion 50, 105005 (2010).
[10] A. Hubbard, D. Whyte, R. Churchill, I. Cziegler, A. Dominguez, T. Golfinopoulos, J. Hughes, J. Rice, M. Greenwald, N. Howard, B. Lipschultz, E. Marmar, M. Reinke, J. Terry, I. Bespamyatnov, and W. Rowan, "Edge energy transport barrier and turbulence in the I-mode regime on alcator C-mod," Phys. Plasmas 18 (2011).
[11] T. Happel, P. Manz, F. Ryter, M. Bernert, M. Dunne, P. Hennequin, A. Hetzenecker, U. Stroth, G. D. Conway, L. Guimarais, C. Honoré, E. Viezzer, and T. A. U. Team, "The I-mode confinement regime at ASDEX Upgrade: global properties and characterization of strongly intermittent density fluctuations," Plasma Phys. Control. Fusion 59, 014004 (2016).
[12] A. Marinoni, J. C. Rost, M. Porkolab, A. E. Hubbard, T. H. Osborne, A. E. White, D. G. Whyte, T. L. Rhodes, E. M. Davis, D. R. Ernst, K. H. Burrell, and t. D.-D. Team, "Characterization of density fluctuations during the search for an I-mode regime on the DIII-D tokamak," Nucl. Fusion 55, 093019 (2015).
[13] A. E. White, P. Phillips, D. G. Whyte, A. E. Hubbard, C. Sung, J. W. Hughes, A. Dominguez, J. Terry, and I. Cziegler, "Electron temperature fluctuations associated with the weakly coherent mode in the edge of Imode plasmas," Nucl. Fusion 51, 113005 (2011).
[14] P. H. Diamond, A. Hasegawa, and K. Mima, "Vorticity dynamics, drift wave turbulence, and zonal flows: a look back and a look ahead," Plasma Phys. Control. Fusion 53, 124001 (2011).

[15] W. W. Xiao, C. Y. Wang, J. X. Zhu, N. Wali, K. Wang, Z. M. Sheng, and G. Y. Fu, "Observation of a nonlinear phenomenon of the density fluctuations on zheda plasma experiment device (ZPED)," AIP Adv. 9, 075026 (2019).
[16] R. L. Burton, S. G. DelMedico, and J. C. Andrews, "Application of a quadruple probe technique to MPD thruster plume measurements," J. Propul. Power 9, 771–777 (1993).
[17] A. I. Smolyakov, P. H. Diamond, and M. V. Medvedev, "Role of ion diamagnetic effects in the generation of large scale flows in toroidal ion temperature gradient mode turbulence," Phys. Plasmas 7, 3987–3992 (2000).
[18] S. Ghosh, P. K. Chattopadhyay, J. Ghosh, and D. Bora, "RF compensation of single Langmuir probe in low density helicon plasma," Fusion Eng. Des. 112, 915–918 (2016).
[19] J. Ma, W. Xiao, C. Wang, W. Niaz, and W. Zhong, "Plasma response associated with external magnetic perturbation fields in a linear plasma device," to be submitted (2023).
[20] M. N. Saha, "LIII. Ionization in the solar chromosphere," The London, Edinburgh, and Dublin Philosophical Magazine and Journal of Science 40, 472–488 (1920).
[21] M. N. Saha, "Versuch einer Theorie der physikalischen Erscheinungen bei hohen Temperaturen mit Anwendungen auf die Astrophysik," Z. Physik 6, 40–55 (1921).
[22] S. J. Levinson, J. M. Beall, E. J. Powers, and R. D. Bengtson, "Space/time statistics of the turbulence in a tokamak edge plasma," Nucl. Fusion 24, 527 (1984).
[23] Y. Ren, W. Guttenfelder, S. Kaye, E. Mazzucato, R. Bell, A. Diallo, C. Domier, B. LeBlanc, K. Lee, M. Podesta, D. Smith, and H. Yuh, "Electron-scale turbulence spectra and plasma thermal transport responding to continuous E×B shear ramp-up in a spherical tokamak," Nucl. Fusion 53, 083007 (2013).
[24] Z. Yan, G. R. McKee, R. Fonck, P. Gohil, R. J. Groebner, and T. H. Osborne, "Observation of the L-H confinement bifurcation triggered by a turbulence-driven shear flow in a tokamak plasma," Phys. Rev. Lett. 112, 125002 (2014).
[25] C. Riccardi, D. Xuantong, M. Salierno, L. Gamberale, and M. Fontanesi, "Experimental analysis of drift waves destabilization in a toroidal plasma," Phys. Plasmas 4, 3749–3758 (1997).
[26] T. Gorler and F. Jenko, "Scale separation between electron and ion thermal transport," Phys. Rev. Lett. 100, 185002 (2008).
[27] W. Horton, "Drift waves and transport," Rev. Mod. Phys. 71, 735–778 (1999).
[28] F. Halpern and P. Ricci, "Velocity shear, turbulent saturation, and steep plasma gradients in the scrape-off layer of inner-wall limited tokamaks," Nucl. Fusion 57, 034001 (2016).
[29] P. H. Diamond, S.-I. Itoh, K. Itoh, and T. S. Hahm, "Zonal flows in plasmaa review," Rev. Sci. Instrum. 47, R35 (2005).
[30] A. V. Latyshev and A. A. Yushkanov, "Behavior of a plasma with the collision rate proportional to the electron velocity in an external electric field," Theor. Math. Phys. 153, 1697–1708 (2007).
[31] A. Hubbard, T. Osborne, F. Ryter, M. Austin, L. B. Orte, R. Churchill, I. Cziegler, M. Fenstermacher, R. Fischer, S. Gerhardt, R. Groebner, P. Gohil, T. Happel, J. Hughes, A. Loarte, R. Maingi, P. Manz, A. Marinoni, E. Marmar, R. McDermott, G. McKee, T. Rhodes, J. Rice, L. Schmitz, C. Theiler, E. Viezzer, J. Walk, A. White, D. Whyte, S. Wolfe, E. Wolfrum, Z. Yan, A. U. the Alcator C-Mod, and D.-D. Teams, "Multi-device studies of pedestal physics and confinement in the i-mode regime," Nucl. Fusion 56, 086003 (2016).

[32] H. Wang, G. Xu, H. Guo, B. Wan, N. Yan, S. Ding, R. Chen, W. Zhang, L. Wang, S. Liu, L. Shao, L. Chen, Y. Liu, Y. Li, G. Hu, and N. Zhao, “Observation of a quasi-coherent high-frequency electromagnetic mode at the pedestal region in east rf-dominant h-modes,” Nucl. Fusion 54, 043014 (2014).
[33] F. Ryter, R. Fischer, J. Fuchs, T. Happel, R. McDermott, E. Viezzer, E. Wolfrum, L. B. Orte, M. Bernert, A. Burckhart, S. da Graça, B. Kurzan, P. McCarthy, T. Pütterich, W. Suttrop, M. Willensdorfer, and the ASDEX Upgrade Team, “I-mode studies at asdex upgrade: L-i and i-h transitions, pedestal and confinement properties,” Nucl. Fusion 57, 016004 (2016).
[34] X. Feng, A. Liu, C. Zhou, Z. Liu, M. Wang, G. Zhuang, X. Zou, T. Wang, Y. Zhang, J. Xie, H. Liu, T. Zhang, Y. Liu, Y. Duan, L. Hu, G. Hu, D. Kong, S. Wang, H. Zhao, Y. Li, L. Shao, T. Xia, W. Ding, T. Lan, H. Li, W. Mao, W. Liu, X. Gao, J. Li, S. Zhang, X. Zhang, Z. Liu, C. Qu, S. Zhang, J. Zhang, J. Ji, H. Fan, and X. Zhong, “I-mode investigation on the experimental advanced superconducting tokamak,” Nucl. Fusion 59, 096025 (2019).
[35] I. Holod, D. Fulton, and Z. Lin, “Microturbulence in diii-d tokamak pedestal. ii. electromagnetic instabilities,” Nucl. Fusion 55, 093020 (2015).
[36] H.-H. Wang, Y.-W. Sun, T.-H. Shi, S. Gu, Y.-Q. Liu, Q. Ma, Q. Zang, K.- Y. He, J.-P. Qian, B. Shen, D.-L. Chen, N. Chu, M.-N. Jia, J. Ren, Z.-P. Luo, Q.-P. Yuan, Y. Wang, B.-J. Xiao, Z.-C. Sheng, M.-H. Li, X.-Z. Gong, L. Zeng, and E. contributors, “Toroidal field and q95 scalings on error field penetration in east,” Nucl. Fusion 60, 126008 (2020).
[37] X.Z. Gong, B.N. Wan, J.G. Li, J.P. Qian, E.Z. Li, F.K. Liu, Y.P. Zhao, M. Wang, H.D. Xu, A.M. Garofalo, A. Ekedah, S.Y. Ding, J. Huang, L. Zhang, Q. Zang, H.Q. Liu, L. Zeng, S.Y. Lin, B. Shen, B. Zhang, L.M. Shao, B.J. Xiao, J.S. Hu, C.D. Hu, L.Q. Hu, L. Wang, Y.W. Sun, G.S. Xu, Y.F. Liang, N. Xiang and EAST Team. Plasma Sci. Technol. 19, 032001 (2017).
[38] Y. Liu, Z. Liu, A. Liu, C. Zhou, X. Feng, Y. Yang, T. Zhang, T. Xia, H. Liu, M. Wu, X. Zou, D. Kong, H. Li, J. Xie, T. Lan, W. Mao, S. Zhang, W. Ding, G. Zhuang, and W. Liu, “Power threshold and confinement of the i-mode in the east tokamak,” Nucl. Fusion 60, 082003 (2020).
[39] S. Kumar, K. Gopal, and D. N. Gupta, “Proton acceleration from overdense plasma target interacting with shaped laser pulses in the presence of preplasmas,” Rev. Sci. Instrum. 61, 085001 (2019).
[40] C. Maggi, R. Groebner, N. Oyama, R. Sartori, L. Horton, A. Sips, W. Suttrop, the ASDEX Upgrade Team, A. Leonard, T. Luce, M. Wade, the DIIID Team, Y. Kamada, H. Urano, the JT-60U Team, Y. Andrew, C. Giroud, E. Joffrin, E. de la Luna, E.-J. C. for the Pedestal, E. Physics, and the Steady State Operation Topical Groups of the ITPA, “Characteristics of the h-mode pedestal in improved confinement scenarios in asdex upgrade, diiid, jet and jt-60u,” Nucl. Fusion 47, 535 (2007).
[41] Y. Huang, T. Xia, X. Xu, D. Kong, Y. Wang, Y. Ye, Z. Qian, Q. Zang, M. Wu, Y. Chu, H. Liu, B. Gui, X. Xiao, and D. Zhang, “Nonlinear simulation and energy analysis of the east coherent mode,” Nucl. Fusion 60, 026014 (2020).
[42] T. Golfinopoulos, B. LaBombard, D. Brunner, J. Terry, S. Baek, P. Ennever, E. Edlund, W. Han, W. Burke, S. Wolfe, J. Irby, J. Hughes, E. Fitzgerald, R. Granetz, M. Greenwald, R. Leccacorvi, E. Marmar, S. Pierson, M. Porkolab, R. Vieira, S. Wukitch, and T. A. C.-M. Team, “Edge transport and mode structure of a qcm-like fluctuation driven by the shoelace antenna,” Nucl. Fusion 58, 056018 (2018).

[43] L. Schmitz, G. Wang, J. C. Hillesheim, T. L. Rhodes, W. A. Peebles, A. E. White, L. Zeng, T. A. Carter, and W. Solomon, “Detection of zonal flow spectra in DIII-D by a dual-channel Doppler backscattering systema),” Rev. Sci. Instrum. 79 (2008).
[44] P. Manz, T. Happel, F. Ryter, M. Bernert, G. Birkenmeier, G. Conway, M. Dunne, L. Guimarais, P. Hennequin, A. Hetzenecker, C. Honoré, P. Lauber, M. Maraschek, V. Nikolaeva, D. Prisiazhniuk, U. Stroth, E. Viezzer, and T. A. U. Team, “Turbulence characteristics of the i-mode confinement regime in asdex upgrade,” Nucl. Fusion 57, 086022 (2017).
[45] S. R. Haskey, A. Ashourvan, S. Banerjee, K. Barada, E. A. Belli, A. Bortolon, J. Candy, J. Chen, C. Chrystal, B. A. Grierson, R. J. Groebner, F. M. Laggner, M. Knolker, G. J. Kramer, M. R. Major, G. Mckee, G. M. Staebler, Z. Yan, and M. A. Van Zeeland, “Ion thermal transport in the H-mode edge transport barrier on DIII-D,” Phys. Plasmas 29 (2022).
[46] U. Plank, T. Pütterich, C. Angioni, M. Cavedon, G. D. Conway, R. Fischer, T. Happel, A. Kappatou, R. M. McDermott, P. A. Schneider, G. Tardini, M. Weiland, and A. U. team, “H-mode power threshold studies in mixed ion species plasmas at asdex upgrade,” Nucl. Fusion 60, 074001 (2020).
[47] F. Ryter, S. Rathgeber, L. B. Orte, M. Bernert, G. Conway, R. Fischer, T. Happel, B. Kurzan, R. McDermott, A. Scarabosio, W. Suttrop, E. Viezzer, M. Willensdorfer, E. Wolfrum, and the ASDEX Upgrade Team, “Survey of the h-mode power threshold and transition physics studies in asdex upgrade,” Nucl. Fusion 53, 113003 (2013).
[48] A. Loarte, J. W. Hughes, M. L. Reinke, J. L. Terry, B. LaBombard, D. Brunner, M. Greenwald, B. Lipschultz, Y. Ma, S. Wukitch, and S. Wolfe, “High confinement/high radiated power H-mode experiments in Alcator C-Mod and consequences for International Thermonuclear Experimental Reactor (ITER) QDT=10 operationa),” Phys. Plasmas 18 (2011).
[49] M. Reinke, D. Brunner, T. Golfinopoulos, A. Hubbard, J. Hughes, A. Kuang, B. LaBombard, E. Marmar, R. Mumgaard, J. Terry, J. Lore, J. Canik, I. Cziegler, and A. C.-M. Team, “Radiative heat exhaust in alcator c-mod i-mode plasmas,” Nucl. Fusion 59, 046018 (2019).
[50] H.J. Kunze, Introduction to Plasma Spectroscopy, 1st ed. (Springer Berlin, Heidelberg, 2009).
[51] I. H. Hutchinson, Principles of Plasma Diagnostics, 2nd ed. (Cambridge University Press, 2002)